

# Spin-Exchange Induced Spillover on Poor Man's Majoranas in Minimal Kitaev Chains

J.E. Sanches,<sup>1,\*</sup> L.T. Lustosa,<sup>1</sup> L.S. Ricco,<sup>2</sup> H. Sigurðsson,<sup>2,3</sup>  
M. de Souza,<sup>4</sup> M.S. Figueira,<sup>5</sup> E. Marinho Jr.,<sup>1,†</sup> and A.C. Seridonio<sup>1,‡</sup>

<sup>1</sup>*São Paulo State University (Unesp), School of Engineering,  
Department of Physics and Chemistry, 15385-007, Ilha Solteira-SP, Brazil*  
<sup>2</sup>*Science Institute, University of Iceland, Dunhagi-3, IS-107, Reykjavik, Iceland*

<sup>3</sup>*Institute of Experimental Physics, Faculty of Physics,  
University of Warsaw, ulica Pasteura 5, PL-02-093 Warsaw, Poland*

<sup>4</sup>*São Paulo State University (Unesp), IGCE, Department of Physics, 13506-970, Rio Claro-SP, Brazil*

<sup>5</sup>*Instituto de Física, Universidade Federal Fluminense, 24210-340, Niterói, Rio de Janeiro, Brazil*

The “Poor Man’s Majoranas” (PMMs) [Phys. Rev. B 86, 134528 (2012)] devoid of topological protection can “spill over” from one edge into another of the minimal Kitaev chain when perturbed electrostatically. As aftermath, this leads to a delocalized Majorana fermion (MF) at both the edges. Additionally, according to recent differential conductance measurements in a pair of superconducting and spinless quantum dots (QDs), such a PMM picture was brought to reality [Nature 614, 445 (2023) and Nature 630, 329 (2024)]. Based on this scenario, we propose the spillover of the PMM when its QD is exchange coupled to a quantum spin  $S$ . We show that if this QD is perturbed by the exchange coupling  $J$ , solely the half  $2S + 1$  ( $2S + 2$ ) of the fine structure stays explicit for a fermionic (bosonic)  $S$ . Concurrently, the other half squeezes itself as the delocalized MF zero-mode. Particularly, turning-off the superconductivity the multiplicity  $2S + 1$  holds regardless the spin statistics. Meanwhile, the PMM spillover induced by  $J$  becomes a statistics dependent effect. Hence, our findings contribute to the comprehension of spin-phenomena interplay with superconductivity in minimal Kitaev chains, offering insights for future quantum computing devices hosting PMMs.

## I. INTRODUCTION

Predicted by Ettore Majorana in 1937, from a particular solution of the Dirac equation, Majorana Fermions (MFs) are particles identical to their antiparticles [1]. These particles were never observed in experiments. However, in condensed matter, they can manifest as quasiparticle excitations called Majorana bound states (MBSs), which appear as zero-energy modes at the edges of topological superconductors [2–27]. Theoretically, the appearance of these MBSs can be understood through the Kitaev toy model [28], which describes a one-dimensional spinless chain with a  $p$ -wave superconducting pairing symmetry. In this model, MBSs emerge as topologically protected, non-local states located at opposite ends of the chain. In the experimental scenario, the achievement of such quasiparticles is still challenging. Thus, MBSs are expected to be the building blocks for the highly-pursued fault-tolerant quantum computing [2, 23, 29]. Consequently, the last decade has witnessed a plethora of theoretical and experimental efforts to explore potential MBS hosts as a basis for cutting-edge quantum computing systems [2, 4, 21, 23, 28–33].

Realizations of the Kitaev chain have been theoretically proposed and experimentally implemented in hybrid setups that combine Zeeman fields, spin-orbit interaction (SOI), and  $s$ -wave superconducting proximity effects [2, 29]. Examples include semiconducting nanowires

with strong Rashba SOI, such as GaAs and InSb, proximitized by conventional  $s$ -wave superconductors [21, 25–27, 29, 30, 34, 35], as well as one-dimensional magnetic chains deposited also on conventional superconductors [8, 9, 14, 33, 36–45], all serving as experimental platforms for hosting MBSs.

Despite clear theoretical frameworks for realizing MBSs in the laboratory, their detection remains challenging, as other phenomena can mimic MBS tunneling transport signatures. Factors such as disorder and zero-energy-pinned Andreev reflections [2, 23] can, for instance, replicate the zero-energy behavior of topological MBSs in a topologically trivial regime, hampering an unambiguous identification. Noteworthy, researchers from Microsoft have claimed recently the realization of an architecture for a topological quantum computer, but with interferometric measurements unable to fully distinguish topological from trivial end states [46].

As aftermath of several accomplishment issues to manufacture a long Kitaev topological wire, we focus on a simpler and experimentally more accessible alternative to hybrid nanowires and magnetic atom chains, such as linear arrays of quantum dots (QDs) with superconductivity, which have emerged as a promising approach to realize shorter Kitaev chains [47–49]. This concept was first proposed in seminal works by Jay D. Sau and S. Das Sarma [50] and by M. Leijnse and K. Flensberg [51], with the latter authors coining the term “Poor Man’s Majoranas” (PMMs) for MBSs in these QD chains, due to their lack of topological protection [51–57]. Recent experimental realizations on two [47, 48] and three QD arrays [49] have revealed electronic transport signatures consistent with the presence of PMMs.

\* corresponding author: jose.sanches@unesp.br

† corresponding author: enesio.marinho@unesp.br

‡ corresponding author: antonio.seridonio@unesp.br

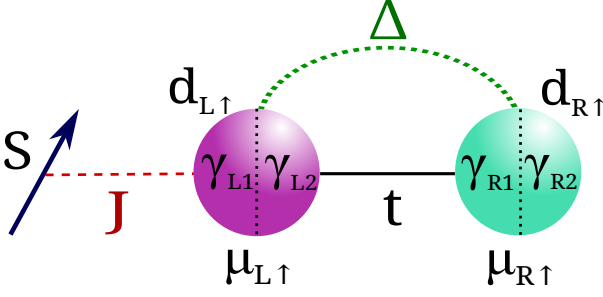


Figure 1. Sketch of the minimal Kitaev chain with a quantum spin  $S$  exchange coupled via  $J$  (red dashed line) to the left quantum dot (purple sphere) with chemical potential  $\mu_{L\uparrow}$ , fermionic operator  $d_{L\uparrow}$ , and the Majorana bound states  $\gamma_{L1}$  and  $\gamma_{L2}$ . For the right quantum dot (green sphere), we have similarly  $\mu_{R\uparrow}$ ,  $d_{R\uparrow}$ ,  $\gamma_{R1}$  and  $\gamma_{R2}$ . Both the quantum dots are connected to each other by electron co-tunneling and crossed Andreev reflection given by  $t$  (black solid line) and  $\Delta$  (green dotted line) terms, respectively. For  $\Delta = t$ ,  $\mu_{L\uparrow} = \mu_{R\uparrow} = 0$  and  $J \neq 0$ , the spillover of the “Poor Man’s Majorana”  $\gamma_{L1}$  yields a delocalized Majorana fermion zero-mode from the squeezing of the half  $2S+1$  ( $2S+2$ ) of the fine structure due to a fermionic (bosonic)  $S$ . Without crossed Andreev reflection, we have the multiplicity  $2S+1$  statistics independent. With crossed Andreev reflection, the dependence on  $S$  allows to distinguish the spin statistics.

Particularly, in a system of two spin-polarized semiconductor QDs coupled via an  $s$ -wave superconductor, known as the minimal Kitaev chain [47], PMMs can form when the QDs are grounded and symmetrically linked through electronic co-tunneling (ECT) and crossed Andreev reflection (CAR) processes. At this *sweet spot* [51], the PMMs emerge as non-local states, spatially separated across the two QDs, similar to conventional MBSs. However, without topological protection, a perturbation to one QD, such as an applied electrostatic potential, induces the PMM at that dot to “spill over” into the other QD [51], resulting in Majorana quasiparticle components in both dots.

Interestingly enough, the absence of topological protection of the PMMs is indeed a trump, favoring the initialization and readout of a PMM-based qubit state [53]. In opposing, perfect MBSs require the break down of the topological protection to be manipulated as a qubit state [58–60]. Thus, due to the relative easy way of state preparation and access via PMMs, braiding and fusion protocols that employ two PMM setups as *Majorana* qubits (four *Majoranas* to compose a two-level system) in a similar architecture to the Tetron qubit from Microsoft [61], have been proposed to verify non-Abelian Physics [53]. This is allowed by the qubit representation, which is based on the fermion parity [51, 62], i.e., the vacuum (even) or single occupied (odd) states from the ordinary fermion made by a pair of PMMs, whose characterization strongly depends on the *Majorana* quality (*Majorana* polarization), a measure of the degree of non-

locality of these PMMs over the host QDs [54]. A detailed discussion on these concepts and near-future experiments covering PMMs can be found in Ref. [53].

In this work, we benefit from the PMMs lack of topological protection to shown that the minimal Kitaev chain is useful to distinguish between fermionic and bosonic spin statistics. We reveal that the PMM exhibits the spillover characteristic if its QD is exchange coupled to a quantum spin. By perturbing this QD via variations of the exchange coupling, the delocalized MF zero-mode arising from the PMM spillover stays decoupled from the half of the fine structure, which is given by  $2S+1$  ( $2S+2$ ) due to a fermionic (bosonic) spin  $S$ . Therefore, the other half then squeezes the mode at zero energy and ensures its pinning there. As the fine structure changes with the statistics of  $S$  in the presence of CAR, the PMM spillover by the exchange coupling is then revealed as a statistics dependent phenomenon. Our findings shed light on the spillover mechanism of PMMs based on a quantum spin, thus opening novel possibilities for spin-related and quantum computing devices.

## II. THE MODEL

We consider the system schematically shown by Fig.1 inspired in the experiments reported by Refs.[47, 48]. Distinctly, we account for the fine structure due to a quantum spin  $S$ . The simplest way to introduce such is via the *Ising-like* Hamiltonian  $JS^z s^z$  [63]. To that end, we adopt the exchange term  $J$  between the *spin-z* operators  $S^z = \sum_m m|m\rangle\langle m|$ , wherein  $m = [-S, -S+1, \dots, S-1, S]$ , and  $s^z = \frac{1}{2} \sum_{\sigma} \sigma d_{L\sigma}^\dagger d_{L\sigma}$  for the quantum spin  $S$  and left QD, respectively, with  $d_{L\sigma}^\dagger$  ( $d_{L\sigma}$ ) as the creation (annihilation) operator and  $\sigma = \pm 1$  ( $\uparrow, \downarrow$ ). For the right QD, we have  $d_{R\sigma}^\dagger$  ( $d_{R\sigma}$ ).

The QDs are found within the spinless regime, where we arbitrary choose the spin-up channel  $\sigma = \uparrow$  as relevant, due to an imposed large Zeeman splitting. Such a dimer of QDs then constitutes the minimal Kitaev chain, being the QDs linked to each other by means of ECT and CAR mechanisms, described by the hopping  $t$  and superconducting pairing  $\Delta$  terms, respectively. This scenario is mimicked by the effective Hamiltonian

$$\mathcal{H} = (\mu_{L\uparrow} + \frac{J}{2} S^z) d_{L\uparrow}^\dagger d_{L\uparrow} + \mu_{R\uparrow} d_{R\uparrow}^\dagger d_{R\uparrow} + (t d_{L\uparrow}^\dagger d_{R\uparrow}^\dagger + \Delta d_{L\uparrow}^\dagger d_{R\uparrow} + \text{H.c.}), \quad (1)$$

where  $\mu_{L\uparrow}$  ( $\mu_{R\uparrow}$ ) represents the chemical potential for the QD  $\alpha = L, R$ . Both the electronic operators of the chain can be expressed in the MBS basis  $\gamma_{L1(L2)}$  and  $\gamma_{R1(R2)}$  for the left and the right QDs, respectively. To perform such, it is imperative to evoke the relations  $d_{L\uparrow} = (\gamma_{L1} + i\gamma_{L2})/\sqrt{2}$  and  $d_{R\uparrow} = (\gamma_{R1} + i\gamma_{R2})/\sqrt{2}$ , which yield

$$\mathcal{H} = (\mu_{L\uparrow} + \frac{J}{2} S^z) (\frac{1}{2} + i\gamma_{L1}\gamma_{L2}) + \mu_{R\uparrow} (\frac{1}{2} + i\gamma_{R1}\gamma_{R2}) + i(\Delta - t)\gamma_{L1}\gamma_{R2} + i(\Delta + t)\gamma_{L2}\gamma_{R1}, \quad (2)$$

from where the “Majorana chain regime”  $t = \Delta$  emerges, being characterized by a *tight-binding-like* Hamiltonian comprising the *Majoranas* of the system following the chain sequence  $\gamma_{L1}, \gamma_{L2}$  and  $\gamma_{R1}$  (MF trimer) or  $\gamma_{L2}$  and  $\gamma_{R1}$  (MF dimer). In the *sweet spot*[51], a limiting case within the “Majorana chain regime” with the constraints  $\mu_{\alpha\uparrow} = \mu_{\bar{\alpha}\uparrow} = J = 0$ , wherein  $\bar{\alpha} = L(R)$  corresponds to the opposite QD  $\alpha = R(L)$ , spatially isolated PMMs  $\gamma_{L1}$  and  $\gamma_{R2}$  appear at the left and right QDs, respectively[47, 48, 51].

We call particular attention to the exchange term  $J$  that plays the role of an effective chemical potential on the left QD. It means that beyond the gate voltage variations attached to the QD triggering the PMM spillover into the opposite QD, similar behavior is expected to occur due to  $J$ . However, as the quantum spin  $S$  can be fermionic or bosonic, we shall see peculiar transition spectra depending on the spin statistics and interplay with the superconducting pairing  $\Delta$ .

In which concerns quantum computing aspects of PMMs, in Ref. [53] a protocol to initialize a PMM-based qubit state via the detuning of both the energy levels of the QDs is deeply discussed and can be, in principle, extended to our system. As the exchange  $J$  allows the tuning of the left QD energy with intricate spin statistics dependence, a second exchange term, let us say  $J_R$ , from an extra spin coupled to the right QD, not solely would fulfill the QDs detuning requirement, but would bring novel possibilities due to the *Ising-like* Hamiltonians of the system. However, we let the exploration of adding a new spin to the system to be done elsewhere. Here, we focus on theoretical spectral analysis and tunneling spectroscopic tool, revealing that Kitaev dimers with PMM spillover due to an exchange coupling, can be employed as a detector of the spin statistics from a quantum spin.

### A. Spectral Analysis

In order to describe the spillover of PMMs, the evaluation of energy dependent retarded Green’s functions (GFs) for the QDs  $\alpha$  are timely. To this end, we should consider the ordinary spectral densities  $\mathcal{A}_{d_{\alpha\uparrow}d_{\alpha\uparrow}^\dagger}(\omega) = (-1/\pi)\text{Im}\langle\langle d_{\alpha\uparrow}; d_{\alpha\uparrow}^\dagger \rangle\rangle$  and  $\mathcal{A}_{d_{\alpha\uparrow}^\dagger d_{\alpha\uparrow}}(\omega) = (-1/\pi)\text{Im}\langle\langle d_{\alpha\uparrow}^\dagger; d_{\alpha\uparrow} \rangle\rangle$ , where  $\langle\langle A; B \rangle\rangle$  stands for the corresponding GF. The anomalous GFs  $\mathcal{A}_{d_{\alpha\uparrow}^\dagger d_{\alpha\uparrow}^\dagger}(\omega) = (-1/\pi)\text{Im}\langle\langle d_{\alpha\uparrow}^\dagger; d_{\alpha\uparrow}^\dagger \rangle\rangle$  and  $\mathcal{A}_{d_{\alpha\uparrow} d_{\alpha\uparrow}}(\omega) = (-1/\pi)\text{Im}\langle\langle d_{\alpha\uparrow}; d_{\alpha\uparrow} \rangle\rangle$  should be taken into account too. As shown below, they determine the MBS component  $\mathcal{A}_{\gamma_{\alpha j}}(\omega) = (-1/\pi)\text{Im}\langle\langle \gamma_{\alpha j}; \gamma_{\alpha j} \rangle\rangle$  of the QD. From  $\gamma_{L1(L2)}$  and  $\gamma_{R1(R2)}$ , we obtain the GF as follows

$$\begin{aligned} \langle\langle \gamma_{\alpha j}; \gamma_{\alpha j} \rangle\rangle &= \frac{1}{2}[\langle\langle d_{\alpha\uparrow}; d_{\alpha\uparrow}^\dagger \rangle\rangle + \langle\langle d_{\alpha\uparrow}^\dagger; d_{\alpha\uparrow} \rangle\rangle \\ &+ \epsilon_j(\langle\langle d_{\alpha\uparrow}^\dagger; d_{\alpha\uparrow}^\dagger \rangle\rangle + \langle\langle d_{\alpha\uparrow}; d_{\alpha\uparrow} \rangle\rangle)], \quad (3) \end{aligned}$$

where  $\epsilon_j = +1, -1$  for  $j = 1, 2$ . Thus, the task of calculating the GFs of Eq.(3) can be achieved via the standard equation-of-motion (EOM) approach[64], which is summarized as

$$(\omega + i\Gamma)\langle\langle A; B \rangle\rangle = \langle\langle [A, B]_+ \rangle\rangle + \langle\langle [A, \mathcal{H}]; B \rangle\rangle, \quad (4)$$

where  $\Gamma$  mimics the natural broadening, supposed to be symmetric for simplicity, arising from the outside environment. By applying the EOM technique to Eq.(1) for  $t \neq \Delta$  we then find

$$\langle\langle d_{\alpha\uparrow}; d_{\alpha\uparrow}^\dagger \rangle\rangle = \frac{1}{2S+1} \sum_m \frac{1}{\omega + i\Gamma - \mu_{\alpha\uparrow} - \frac{Jm}{2}\delta_{\alpha L} - \Sigma_\alpha^+}, \quad (5)$$

$$\langle\langle d_{\alpha\uparrow}^\dagger; d_{\alpha\uparrow} \rangle\rangle = \frac{1}{2S+1} \sum_m \frac{1}{\omega + i\Gamma + \mu_{\alpha\uparrow} + \frac{Jm}{2}\delta_{\alpha L} - \Sigma_\alpha^-}, \quad (6)$$

$$\langle\langle d_{\alpha\uparrow}^\dagger; d_{\alpha\uparrow}^\dagger \rangle\rangle = \frac{\eta_\alpha}{2S+1} \sum_m \frac{2t\Delta K_\alpha^-}{\omega + i\Gamma + \mu_{\alpha\uparrow} + \frac{Jm}{2}\delta_{\alpha L} - \Sigma_\alpha^-}, \quad (7)$$

and

$$\langle\langle d_{\alpha\uparrow}; d_{\alpha\uparrow} \rangle\rangle = \frac{\eta_\alpha}{2S+1} \sum_m \frac{2t\Delta K_\alpha^+}{\omega + i\Gamma - \mu_{\alpha\uparrow} - \frac{Jm}{2}\delta_{\alpha L} - \Sigma_\alpha^+}, \quad (8)$$

where we used  $\langle\langle A; B \rangle\rangle = \sum_m \langle\langle A | m \rangle \langle m |; B \rangle\rangle$ , the thermal average  $\langle |m\rangle \langle m| \rangle = \frac{1}{2S+1}$ ,  $\delta_{\alpha L}$  as the Kronecker Delta and  $\eta_\alpha = -1, +1$  for  $\alpha = L, R$ , respectively. The self-energy correction due to the couplings  $t, \Delta$  and  $J$  is  $\Sigma_\alpha^\pm = \tilde{K}_\alpha^\pm + (2t\Delta)^2 K_\alpha^\pm$ , with

$$\tilde{K}_\alpha^\pm = \frac{(\omega + i\Gamma)(t^2 + \Delta^2) \pm (\mu_{\alpha\uparrow} + \frac{Jm}{2}\delta_{\alpha L})(t^2 - \Delta^2)}{(\omega + i\Gamma)^2 - (\mu_{\alpha\uparrow} + \frac{Jm}{2}\delta_{\alpha L})^2}, \quad (9)$$

$$K_\alpha = \frac{\omega + i\Gamma}{(\omega + i\Gamma)^2 - (\mu_{\alpha\uparrow} + \frac{Jm}{2}\delta_{\alpha L})^2} \quad (10)$$

and

$$K_\alpha^\pm = \frac{K_{\bar{\alpha}}}{\omega + i\Gamma \pm \mu_{\alpha\uparrow} \pm \frac{Jm}{2}\delta_{\alpha L} - \tilde{K}_\alpha^\mp}. \quad (11)$$

It is worth mentioning that the expression of Eq.(3) for the *Majorana* GF  $\langle\langle \gamma_{\alpha j}; \gamma_{\alpha j} \rangle\rangle$  wrap ups processes as electron (hole) tunneling  $\langle\langle d_{\alpha\uparrow}; d_{\alpha\uparrow}^\dagger \rangle\rangle$  ( $\langle\langle d_{\alpha\uparrow}^\dagger; d_{\alpha\uparrow} \rangle\rangle$ ) and the corresponding local Andreev reflection  $\langle\langle d_{\alpha\uparrow}^\dagger; d_{\alpha\uparrow}^\dagger \rangle\rangle$  ( $\langle\langle d_{\alpha\uparrow}; d_{\alpha\uparrow} \rangle\rangle$ ) at the QD  $\alpha$ . As the coefficient  $\epsilon_j$  changes sign when the *Majorana* index  $j$  is swapped, the aforementioned transport channels can interfere constructively or destructively depending on the *Majorana* GF

for a fixed QD. In this way, the spectral function  $\mathcal{A}_{\gamma_{\alpha j}}(\omega)$  is expected to exhibit resonant peaks and dips spanned by  $\omega$  and  $J$  for tuned parameters  $t, \Delta$  and  $\mu_{\alpha\uparrow}$ . Interestingly enough, such interference processes lead to different scenarios for the system “*Majorana chain regime*”, such as the MF trimer ( $\gamma_{L1}, \gamma_{L2}$  and  $\gamma_{R1}$ ) and dimer ( $\gamma_{L2}$  and  $\gamma_{R1}$ ), as well as the PMMs ( $\gamma_{L1}$  and  $\gamma_{R2}$ ) in the *sweet spot*. Therefore, the so-called bonding, anti-bonding and non-bonding molecular states, and the zero-mode are due to the quasiparticle interference encoded by  $\mathcal{A}_{\gamma_{\alpha j}}(\omega)$ . We shall see these features in Sec. 3.

## B. Tunneling Spectroscopy

To access experimentally the features of the spectral densities, one should perform a quantum transport evaluation of the system conductance. From a theoretical perspective, we adopt the proposal found in Ref. [65], which consists in flanking a QD by source and drain metallic leads with chemical potentials  $\mu_{\text{Source}}$  and  $\mu_{\text{Drain}}$ , respectively. Thus, we should add to the Hamiltonian of Eq. (1) the terms for the leads and their couplings to the left QD as follows

$$\mathcal{H}_{\text{Total}} = \mathcal{H} + \sum_{\tilde{q}, \mathbf{k}} (\varepsilon_{\mathbf{k}} - \mu_{\tilde{q}}) c_{\tilde{q}\mathbf{k}}^\dagger c_{\tilde{q}\mathbf{k}} + V_L \sum_{\tilde{q}, \mathbf{k}} (c_{\tilde{q}\mathbf{k}}^\dagger d_{L\uparrow} + \text{H.c.}), \quad (12)$$

where the second term stands for the leads with  $\tilde{q} = q = \text{Source}$  ( $\tilde{q} = \bar{q} = \text{Drain}$ ) and in the third part  $V_L$  represents the symmetric QD-lead tunneling term. In this way, the current  $I_q$  can be decomposed into the parts

$$I_q = I_q^{\text{ET}} + I_q^{\text{LAR}} + I_q^{\text{CAR}}, \quad (13)$$

where

$$I_q^{\text{ET}} = \frac{e}{h} \int d\varepsilon \tau_{q\bar{q}}^{\text{ET}}(\varepsilon) [f_q^e(\varepsilon) - f_{\bar{q}}^e(\varepsilon)], \quad (14)$$

$$I_q^{\text{CAR}} = \frac{e}{h} \int d\varepsilon \tau_{q\bar{q}}^{\text{CAR}}(\varepsilon) [f_q^e(\varepsilon) - f_{\bar{q}}^h(\varepsilon)] \quad (15)$$

and

$$I_q^{\text{LAR}} = \frac{e}{h} \int d\varepsilon \tau_{q\bar{q}}^{\text{LAR}}(\varepsilon) [f_q^e(\varepsilon) - f_q^h(\varepsilon)], \quad (16)$$

where  $I_q^{\text{ET}}$  and  $I_q^{\text{CAR}}$  stem from the currents for the electron tunneling (ET) and crossed Andreev reflection (CAR) with occupation probabilities of an electron  $f_q^e(\varepsilon)$  and hole  $f_{\bar{q}}^h(\varepsilon)$  states at lead  $\bar{q}$ , respectively, where  $f_q^j(\varepsilon)$  stands for the Fermi distribution at lead  $q$  and  $j = e(h)$  for the electron (hole) quasiparticle. In the case of the local Andreev reflection (LAR)  $I_q^{\text{LAR}}$ , the hole emission occurs into the same terminal  $q$ , as it depends on  $f_q^h(\varepsilon)$ . Particularly, with the assumption  $\mu_{\text{Source}} = -\mu_{\text{Drain}} = eV/2$

we conclude that  $f_q^e(\varepsilon) = f_{\bar{q}}^h(\varepsilon)$ , which from Eq. (15) results in  $I_q^{\text{CAR}} = 0$  (this not implies in the absence of the system intrinsic CAR given by  $\Delta$  between left and right QDs) and  $I_q = -I_{\bar{q}}$ , whose the transmittance coefficients are determined by  $\tau_{q\bar{q}}^{\text{ET}} = (2S+1)\Gamma_L^2 |\langle\langle d_{L\uparrow}; d_{L\uparrow}^\dagger \rangle\rangle_\omega|^2$  and  $\tau_{q\bar{q}}^{\text{LAR}} = (2S+1)\Gamma_L^2 |\langle\langle d_{L\uparrow}^\dagger; d_{L\uparrow}^\dagger \rangle\rangle_\omega|^2$ , where  $\Gamma_L = 2\pi V_L^2 \rho$  represents the symmetric electron (hole)- QD spectral broadening term and  $\rho$  the lead DOS. Thus, the conductance from the source reservoir reads

$$\mathcal{G}_q = \frac{dI_q}{dV} = \frac{dI_q^{\text{ET}}}{dV} + \frac{dI_q^{\text{LAR}}}{dV}, \quad (17)$$

with

$$\begin{aligned} \frac{dI_q^{\text{ET}}}{dV} &= \frac{e^2}{2h} \frac{1}{T} \int d\varepsilon \tau_{q\bar{q}}^{\text{ET}}(\varepsilon) \{f_q^e(\varepsilon)[1 - f_{\bar{q}}^e(\varepsilon)] \\ &+ f_{\bar{q}}^e(\varepsilon)[1 - f_{\bar{q}}^e(\varepsilon)]\}, \end{aligned} \quad (18)$$

and

$$\begin{aligned} \frac{dI_q^{\text{LAR}}}{dV} &= \frac{e^2}{2h} \frac{1}{T} \int d\varepsilon \tau_{q\bar{q}}^{\text{LAR}}(\varepsilon) \{f_q^e(\varepsilon)[1 - f_q^e(\varepsilon)] \\ &+ f_{\bar{q}}^e(\varepsilon)[1 - f_{\bar{q}}^e(\varepsilon)]\}, \end{aligned} \quad (19)$$

where we employed the identity  $f_q^e(\varepsilon) = f_{\bar{q}}^h(\varepsilon)$  and

$$\frac{\partial f_{q(\bar{q})}^e(\varepsilon)}{\partial V} = \pm \frac{e}{2T} f_{q(\bar{q})}^e(\varepsilon) [1 - f_{q(\bar{q})}^e(\varepsilon)], \quad (20)$$

with  $k_B = 1$ ,  $f_q^e(\varepsilon) = f(\varepsilon - eV/2)$ ,  $f_{\bar{q}}^e(\varepsilon) = f(\varepsilon + eV/2)$  and  $f(x) = 1/(1 + e^{x/T})$ .

As  $\frac{1}{T} f_{q(\bar{q})}^e(\varepsilon) [1 - f_{q(\bar{q})}^e(\varepsilon)] = \left(-\frac{\partial f_{q(\bar{q})}^e(\varepsilon)}{\partial \varepsilon}\right) \rightarrow \delta(\varepsilon \mp eV/2)$  when  $T \rightarrow 0\text{K}$ , then we find

$$\mathcal{G}_{\text{Source}} = \mathcal{G}_{\text{ET}}(eV) + \mathcal{G}_{\text{LAR}}(eV), \quad (21)$$

$$\mathcal{G}_{\text{ET}}(eV) = \frac{e^2}{2h} [\tau_{q\bar{q}}^{\text{ET}}(eV/2) + \tau_{q\bar{q}}^{\text{ET}}(-eV/2)], \quad (22)$$

and

$$\mathcal{G}_{\text{LAR}}(eV) = \frac{e^2}{2h} [\tau_{q\bar{q}}^{\text{LAR}}(eV/2) + \tau_{q\bar{q}}^{\text{LAR}}(-eV/2)] \quad (23)$$

in agreement with Ref. [65]. Before the numerical analysis of Sec. 3, we highlight that the GFs that determine  $\mathcal{G}_{\text{Source}}$  follow the set of Eqs. (5)-(8) with the substitution  $\Gamma \rightarrow \Gamma + \Gamma_L \delta_{\alpha L}$ , due to the coupling between the left QD and source-drain leads.



### III. RESULTS AND DISCUSSION

In Fig.2, we introduce the PMM spillover induced by  $J$ . Experimentally speaking,  $J$  can be tuned by changing the distance between the spin  $S$  site and the leftmost QD. For such an analysis, we first consider the “Majorana chain regime”  $t = \Delta = 1.5$ , with  $\mu_{L\uparrow} = \mu_{R\uparrow} = 0$  in arbitrary units for the fermionic case  $S = 1.5$ , and evaluate the spectral functions spanned by  $\omega$  and  $J$ . Particularly, when  $J = 0$  the *sweet spot* is restored and we have the MF dimer  $\gamma_{L2}$  and  $\gamma_{R1}$  described by  $\mathcal{H} = 2it\gamma_{L2}\gamma_{R1}$ , and the isolated PMMs  $\gamma_{L1}$  and  $\gamma_{R2}$ , once they do not enter into  $\mathcal{H}$ , at the left and right QDs, respectively. However for  $J \neq 0$ , the Hamiltonian turns into  $\mathcal{H} \sim i\frac{J}{2}S^z\gamma_{L1}\gamma_{L2} + 2it\gamma_{L2}\gamma_{R1}$  yielding the MF trimer established by  $\gamma_{L1}, \gamma_{L2}$  and  $\gamma_{R1}$ , which drives the system into the regime where  $\gamma_{L1}$  “spills over” towards  $\gamma_{R1}$ .

To perceive such a scenario, we begin the analysis with  $\mathcal{A}_{\gamma_{L1}}$  and  $\mathcal{A}_{\gamma_{R2}}$  in Figs.2(a) and (e), which due to the  $J = 0$  condition, gives rise to the non-local PMMs  $\gamma_{L1}$  and  $\gamma_{R2}$  (purple line cuts), respectively. These PMMs are represented by the finite and equal amplitudes for the zero-energy mode at  $\omega = 0$ . At  $J = 0$ ,  $\mathcal{A}_{\gamma_{L2}}$  and  $\mathcal{A}_{\gamma_{R1}}$  display a split-peak structure as a function of  $\omega$ , once  $\gamma_{L2}$  and  $\gamma_{R1}$  build the MF dimer (cyan line cuts in Figs.2(b) and (d)). For  $J \neq 0$  and  $\omega \neq 0$ , extra bottom (bonding) and top (anti-bonding) arcs rise in Figs.2(a), (b) and (d) for  $\mathcal{A}_{\gamma_{L1}}, \mathcal{A}_{\gamma_{L2}}$ , and  $\mathcal{A}_{\gamma_{R1}}$ , respectively, as a consequence of the MF trimer formation (green line cuts). In Figs.2(a) and (d) for  $J \neq 0$ , the resonance at  $\omega = 0$  corresponds to the non-bonding state of the MF trimer. Particularly, the multiplicity of arcs is  $2S + 1$  due to the fermionic spin and it corresponds to half of the total fine structure  $2 \times (2S + 1)$  as we shall see in the analysis off the “Majorana chain regime”. The spillover of  $\gamma_{L1}$  on  $\gamma_{R1}$  can be noted in Figs.2(a) and (d), where the unbalance  $\mathcal{A}_{\gamma_{L1}}(0) < \mathcal{A}_{\gamma_{R1}}(0)$  is observed away from  $J = 0$ . In this manner, we reveal that the zero mode of the PMM  $\gamma_{L1}$  “spills over” from its QD into the opposite. Additionally, it means that the zero-mode from a delocalized MF at both the QDs emerges as aftermath of the squeezing of the other half  $2S + 1$ .

Thus, the unbalance also in  $\mathcal{A}_{d_{\alpha\uparrow}d_{\alpha\uparrow}^\dagger}(0) < \mathcal{A}_{d_{\bar{\alpha}\uparrow}d_{\bar{\alpha}\uparrow}^\dagger}(0)$  off  $J = 0$  and the explicit  $2S + 1$  fine structure of Figs.2(c) and (f) consist the hallmarks of the spillover of a PMM in the presence of a fermionic spin.

In order to elucidate the dependence of fine structure on  $S$  and the underlying squeezing mechanism to build the zero-mode of the delocalized MF due to the PMM spillover, in Fig.3 we present  $\mathcal{A}_{d_{L\uparrow}d_{L\uparrow}^\dagger}$  for the case  $\Delta = 0.5t$ , which corresponds to a situation off the “Majorana chain regime”. It is worth mentioning that the exhibition of  $\mathcal{A}_{d_{R\uparrow}d_{R\uparrow}^\dagger}$  is redundant, once it shares the same features observed in  $\mathcal{A}_{d_{L\uparrow}d_{L\uparrow}^\dagger}$ .

Particularly, the anti-crossing point at  $J = 0$  in Figs.3(a) and (b) of the energy levels arise from the existence of two MF dimers, namely  $\gamma_{L2}, \gamma_{R1}$  and  $\gamma_{L1}, \gamma_{R2}$  as

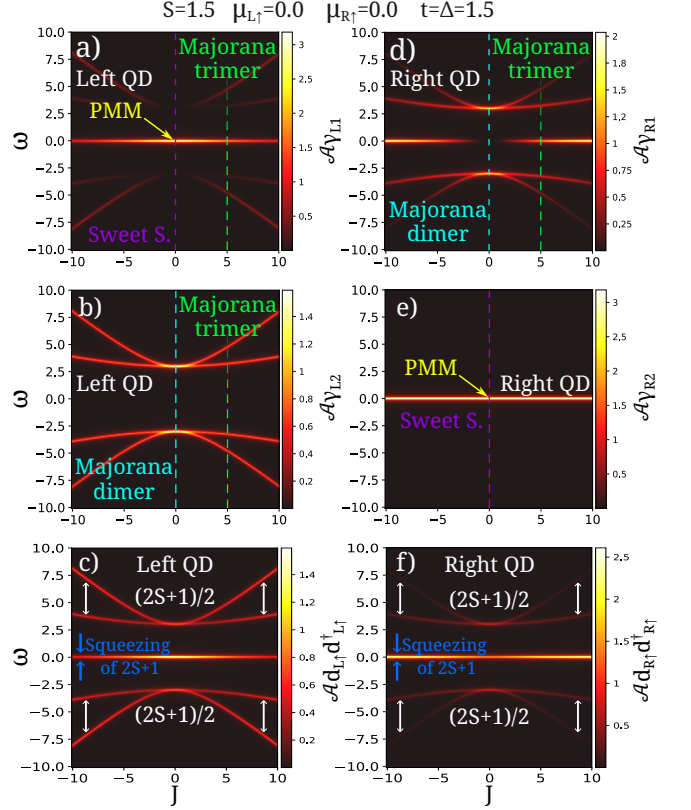


Figure 2. The spillover of the PMM induced by  $J$ . Color maps of  $\mathcal{A}_{d_{\alpha\uparrow}d_{\alpha\uparrow}^\dagger}$  and  $\mathcal{A}_{\gamma_{\alpha j}}$  in the “Majorana chain regime” spanned by  $\omega$  and  $J$  showing that in the presence of the fermionic spin  $S$ ,  $2S + 1$  of the fine structure is the explicit part. The other half  $2S + 1$  squeezes itself at  $\omega = 0$  forming the delocalized MF zero-mode due to the PMM spillover.

aftermath of  $\mathcal{H} = i(\Delta - t)\gamma_{L1}\gamma_{R2} + i(\Delta + t)\gamma_{L2}\gamma_{R1}$ . Thus, the Kitaev dimer with  $\Delta \neq t$  and  $\mu_{\alpha\uparrow} = \mu_{\bar{\alpha}\uparrow} = J = 0$  exhibits a four-peak structure, which is distinct from the typical two (bonding and anti-bonding) of an ordinary molecule with  $\Delta = 0$ , i.e.,  $\mathcal{H} = -it\gamma_{L1}\gamma_{R2} + it\gamma_{L2}\gamma_{R1}$  as can be noted in Figs.3(c) and (d). Therefore, as we can observe in Fig.3(a) for the fermionic spin  $S = 1.5$ ,  $2 \times (2S + 1)$  levels appear as  $|J|$  increases. This set reveals a squeezing trend of the inner fine structure, which delimits precisely  $2S + 1$  levels nearby  $\omega = 0$ , into a delocalized MF zero-mode. We call attention to the pattern of this inner portion of fine structure that precedes the “Majorana chain regime”  $\Delta = t$  of Fig.2, with all these inner levels squeezed at  $\omega = 0$  upon approaching  $\Delta \rightarrow t$ .

In Fig.3(b) for the bosonic spin  $S = 2$ , the multiplicity  $2S + 1$  changes to  $2S + 2$ . It means that the explicit part of the fine structure becomes  $2S + 2$  when  $t = \Delta$  and half of the total spectrum  $2 \times (2S + 2)$  squeezes at  $\omega = 0$ , i.e.,  $2S + 2$ .

To understand such a variation, let us remind that when the CAR is turned-off ( $\Delta = 0$ ), the fine structure  $2 \times (2S + 1)$  takes place and is independent of  $S$ . This appears in Figs.3(c) and (d). As a matter of fact, the

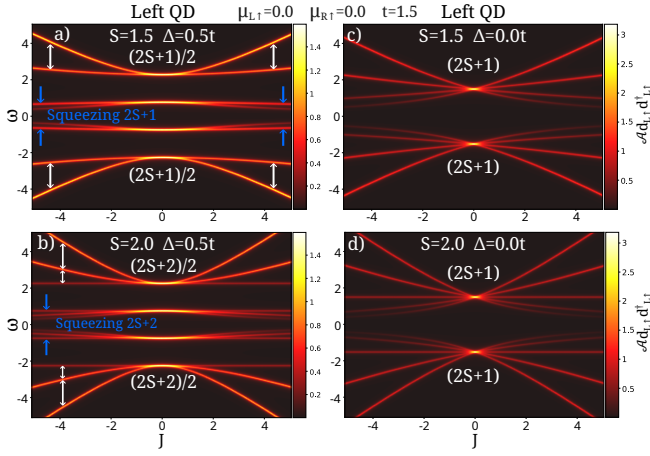


Figure 3. Color map of  $\mathcal{A}_{d_{L\uparrow}d_{L\uparrow}^\dagger}$  off the “Majorana chain regime” spanned by  $\omega$  and  $J$  for: (a) Fermion case  $S = 1.5$ . The total fine structure contains  $2 \times (2S + 1)$  levels as  $|J|$  increases, but the inner half reveals a squeezing into a delocalized MF zero-mode due to the spillover of the PMM. (b) Boson case  $S = 2$ . The entire fine structure is  $2 \times (2S + 2)$  as  $|J|$  increases and the inner half shows the same trend of (a). (c) and (d) exhibit the dimer without CAR ( $\Delta = 0$ ) and the fine structure  $2 \times (2S + 1)$  is statistics independent.

difference between fermions and bosons for  $\Delta \neq 0$  relies on the mirror symmetry of the spectrum around  $\omega = |t|$ . In case of a bosonic  $S$ , the multiplicity  $2S + 1$  is odd and for  $\Delta = 0$  the state  $m = 0$  corresponds to  $\omega = |t|$ , being flanked by  $S$  states. A finite  $\Delta$  [Figs.3(a) and (b)] then splits  $|t|$  into  $|\Delta - t|$  and  $|\Delta + t|$ , thus changing  $2S + 1$  to  $2S + 2$ . As for fermionic  $S$ ,  $2S + 1$  is even and the  $m = 0$  state does not exist, it cannot be split by  $\Delta$  and the multiplicity  $2S + 1$  is maintained as aftermath. Such a behavior can be viewed in the animated plots of the Supplementary Material. Particularly for bosonic  $S$ , notice that the frame  $\Delta = 0.01t$  defines the threshold for the peaks at  $\omega = |t|$  (purple dashed lines) to split into those at  $|\Delta - t|$  (blue lines) and  $|\Delta + t|$  (red lines), which can be seen for instance in the frame  $\Delta = 0.05t$ . In the other hand, there are no peaks at  $\omega = |t|$  to be split for fermionic  $S$ .

Experimentally, one pathway to observe our results consists in performing the tunneling spectroscopy approach of Sec. 2.2. Here, in the simulations, we adopt  $\Gamma_L$  as energy unit and  $\Gamma = 0.01$  in Eqs.(5) and (7) for the left QD with  $\Gamma \rightarrow \Gamma + \Gamma_L \delta_{\alpha L}$ . In this way, in Fig.4(a) we depict the conductance  $\mathcal{G}_{\text{Source}}$  of Eq.(21) spanned by the bias-voltage  $eV$  and  $J$  for the fermionic case  $S = 1.5$ , with  $t = \Delta = 1.5$  and  $\mu_{L\uparrow} = \mu_{R\uparrow} = 0$ . Note that the conductance pattern is qualitatively the same verified in Fig.2(c) for  $\mathcal{A}_{d_{L\uparrow}d_{L\uparrow}^\dagger}$  with explicit multiplicity  $2S + 1$ . Particularly in Fig.4(b), we show the bias-voltage dependence of  $\mathcal{G}_{\text{Source}}$  with  $J = 10$ . In this panel, we clearly observe  $(2S + 1)/2 = 2$  resonant states for  $S = 1.5$  flanking the zero-bias peak, which according to Figs.2 and 3, represent the net effect of the squeezing of the other half of the

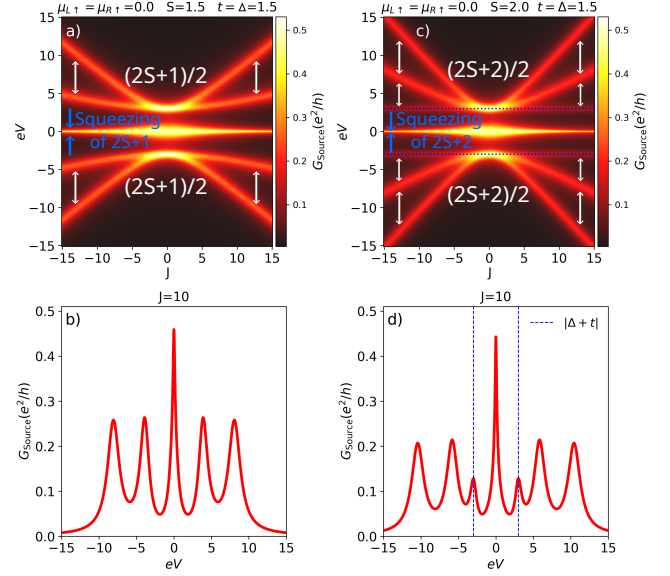


Figure 4. Differential conductance  $\mathcal{G}_{\text{Source}}$  of Eq.(21) as a tunneling spectroscopic tool to detect the spin statistics from a quantum spin with a Kitaev dimer and the PMM spillover due to an exchange coupling  $J$ . (a) Color map of  $\mathcal{G}_{\text{Source}}$  spanned by the bias-voltage  $eV$  and  $J$  for the fermionic case  $S = 1.5$  wherein energy levels bend (arcs) with  $J$  and  $(2S + 1)/2$  side-peaks. (b)  $\mathcal{G}_{\text{Source}}$  versus  $eV$  for  $J = 10$  showing a zero-bias conductance  $\mathcal{G}_{\text{Source}}(0) < e^2/2h$ , which strikes out a truly PMM, being a zero-energy Andreev state. (c) Color map of  $\mathcal{G}_{\text{Source}}$  for the bosonic  $S = 2.0$  wherein low energy levels flanking the zero-bias peak do not bend anymore with  $J$  (flat dashed lines at  $eV = |\Delta + t|$  and  $(2S + 2)/2$  side-peaks. (d)  $\mathcal{G}_{\text{Source}}$  versus  $eV$  for  $J = 10$  also showing a zero-energy Andreev state, but with side-peaks at  $eV = |\Delta + t|$ . The flat levels in (c) represent the hallmark of a bosonic quantum spin.

fine structure as a zero-mode. Additionally, as  $\mathcal{G}_{\text{Source}}(0)$  stays below  $e^2/2h$  we can safely conclude that the zero-energy state does not arise from an isolated MF [65], which in this case would be a truly PMM. Indeed, this zero-energy corresponds to a delocalized MF zero-mode or simply an Andreev state due to the PMM spillover towards the right QD. Noteworthy, to distinguish Figs.4(a) and (b) from a counterpart bosonic case, which has the same number of side-peaks as in the fermionic situation  $S = 1.5$  but with the formula  $(2S + 2)/2 = 2$  for  $S = 1$ , we should inspect if the conductance profile contains resonant states pinned at  $|\Delta + t|$  regardless the strength of the exchange  $J$ . According to the revealed mechanism responsible for the multiplicity change from  $2S + 1$  to  $2S + 2$  for a bosonic quantum spin, the state  $m = 0$ , being centered at  $eV = |t|$ , consists in the unique existent resonant state due to the odd parity of the original fine structure  $2S + 1$  when the superconductivity is absent. Then, the superconductor splits  $eV = |t|$  into  $|\Delta - t|$  and  $|\Delta + t|$  and consequently, it rises the multiplicity. When  $t = \Delta$ , solely the peak positions at  $|\Delta + t| = |2t|$  remain intact upon varying  $J$ , as we can see denoted by dashed lines in

Figs.4(c) and (d). For the even parity of  $2S + 1$  from a fermionic quantum spin, the states  $eV = |t|$  are removed and the superconductor does not have the state  $m = 0$  to be split.

In summary, if the color map of  $\mathcal{G}_{\text{Source}}$  versus  $eV$  and  $J$  shows two flat levels on  $J$  flanking the zero-bias peak such as the marked dashed lines in Fig.4(c), the transition spectrum belongs to a bosonic  $S$  and we should apply the formula “ $2S + 2 = \text{total of peaks}$ , except that from the zero-bias” to figure out the value of  $S$ . Otherwise, if these near-zero energy levels bend with  $J$  (a pair of arcs) in the conductance color map as shown in Fig.4(a), we then change in the left side of the previous formula to  $2S + 1$  and find the corresponding fermionic quantum spin instead.

#### IV. CONCLUSIONS

We demonstrate that in a system of two superconducting, spinless QDs corresponding to the minimal Kitaev chain, the PMM exhibits the spillover effect from one QD to the other when perturbed by an exchange coupling with a quantum spin  $S$ . This effect results in a delocalized MF zero-mode, comprising half of the fine structure induced by the exchange interaction. The remaining fine structure, representing  $2S + 1$  or  $2S + 2$  states, arises from

the fermionic or bosonic nature of the spin, respectively. For a dimer without CAR, this fine structure consistently shows  $2S + 1$  levels, independent of the spin statistics. These findings demonstrate the potential for analyzing minimal Kitaev chains through quantum spin interactions, with implications for spin-related phenomena and quantum computing.

#### V. ACKNOWLEDGMENTS

We thank the Brazilian funding agencies CNPq (Grants. Nr. 302887/2020-2, 303772/2023-9, 311980/2021-0, and 308695/2021-6), the São Paulo Research Foundation (FAPESP; Grant No. 2023/13467-6), Coordenação de Aperfeiçoamento de Pessoal de Nível Superior - Brasil (CAPES) – Finance Code 001 and FAPERJ process Nr. 210355/2018. LSR acknowledges the support from the Icelandic Research Fund (Rannís), Grant No. 239552-051. LSR thanks Unesp for their hospitality. HS acknowledges the project No. 2022/45/P/ST3/00467 co-funded by the Polish National Science Centre and the European Union Framework Programme for Research and Innovation Horizon 2020 under the Marie Skłodowska-Curie grant agreement No. 945339.

- 
- [1] E. Majorana, *Il Nuovo Cimento* (1924-1942) **14**, 10.1007/BF02961314 (1937).
  - [2] P. Marra, *Journal of Applied Physics* **132**, 231101 (2022).
  - [3] E. Vernek, P. H. Penteado, A. C. Seridonio, and J. C. Egues, *Phys. Rev. B* **89**, 165314 (2014).
  - [4] O. Lesser and Y. Oreg, *Journal of Physics D: Applied Physics* **55**, 164001 (2022).
  - [5] F. Pientka, L. I. Glazman, and F. von Oppen, *Phys. Rev. B* **89**, 180505 (2014).
  - [6] Y. Oreg, G. Refael, and F. von Oppen, *Phys. Rev. Lett.* **105**, 177002 (2010).
  - [7] F. Pientka, L. I. Glazman, and F. von Oppen, *Phys. Rev. B* **88**, 155420 (2013).
  - [8] J. Klinovaja, P. Stano, A. Yazdani, and D. Loss, *Phys. Rev. Lett.* **111**, 186805 (2013).
  - [9] S. Nadj-Perge, I. K. Drozdov, B. A. Bernevig, and A. Yazdani, *Phys. Rev. B* **88**, 020407 (2013).
  - [10] L. Fu and C. L. Kane, *Phys. Rev. B* **79**, 161408 (2009).
  - [11] L. Fu and C. L. Kane, *Phys. Rev. Lett.* **100**, 096407 (2008).
  - [12] M. M. Vazifeh and M. Franz, *Phys. Rev. Lett.* **111**, 206802 (2013).
  - [13] S. Nakosai, Y. Tanaka, and N. Nagaosa, *Phys. Rev. B* **88**, 180503 (2013).
  - [14] B. Braunecker and P. Simon, *Phys. Rev. Lett.* **111**, 147202 (2013).
  - [15] A. C. Potter and P. A. Lee, *Phys. Rev. B* **85**, 094516 (2012).
  - [16] S. B. Chung, H.-J. Zhang, X.-L. Qi, and S.-C. Zhang, *Phys. Rev. B* **84**, 060510 (2011).
  - [17] C. W. J. Beenakker, *Rev. Mod. Phys.* **87**, 1037 (2015).
  - [18] M. Sato and S. Fujimoto, *Journal of the Physical Society of Japan* **85**, 072001 (2016).
  - [19] M. Sato and Y. Ando, *Reports on Progress in Physics* **80**, 076501 (2017).
  - [20] A. Haim and Y. Oreg, *Physics Reports* **825**, 1 (2019), time-reversal-invariant topological superconductivity in one and two dimensions.
  - [21] J. Alicea, *Reports on Progress in Physics* **75**, 076501 (2012).
  - [22] C. Beenakker, *Annual Review of Condensed Matter Physics* **4**, 113 (2013).
  - [23] A. S. Karsten Flensberg, Felix von Oppen, *Nature Reviews Materials* **6**, 944 (2021).
  - [24] K. Laubscher and J. Klinovaja, *Journal of Applied Physics* **130**, 081101 (2021).
  - [25] M. T. Deng, S. Vaitiekenas, E. B. Hansen, J. Danon, M. Leijnse, K. Flensberg, J. Nygard, P. Krogstrup, and C. M. Marcus, *Science* **354**, 1557 (2016).
  - [26] V. Mourik, K. Zuo, S. M. Frolov, S. R. Plissard, E. P. A. M. Bakkers, and L. P. Kouwenhoven, *Science* **336**, 1003 (2012).
  - [27] F. Nichele, A. C. C. Drachmann, A. M. Whiticar, E. C. T. O’Farrell, H. J. Suominen, A. Fornieri, T. Wang, G. C. Gardner, C. Thomas, A. T. Hatke, P. Krogstrup, M. J. Manfra, K. Flensberg, and C. M. Marcus, *Phys. Rev. Lett.* **119**, 136803 (2017).
  - [28] A. Y. Kitaev, *Physics-Uspekhi* **44**, 131 (2001).
  - [29] R. Aguado, *LA RIVISTA DEL NUOVO CIMENTO* **40**, 523 (2017).

- [30] S. R. Elliott and M. Franz, *Rev. Mod. Phys.* **87**, 137 (2015).
- [31] M. Leijnse and K. Flensberg, *Semiconductor Science and Technology* **27**, 124003 (2012).
- [32] T. D. Stanescu and S. Tewari, *Journal of Physics: Condensed Matter* **25**, 233201 (2013).
- [33] B. Jack, Y. Xie, and A. Yazdani, *Nature Reviews Physics* **3**, 2522 (2021).
- [34] R. M. Lutchyn, J. D. Sau, and S. Das Sarma, *Phys. Rev. Lett.* **105**, 077001 (2010).
- [35] M. Aghaee and *et al.* (Microsoft Quantum), *Phys. Rev. B* **107**, 245423 (2023).
- [36] R. Pawlak, M. Kisiel, J. Klinovaja, T. Meier, S. Kawai, T. Glatzel, D. Loss, and E. Meyer, *npj Quantum Information* **2**, 10.1038/npjqi.2016.35 (2016).
- [37] M. Ruby, F. Pientka, Y. Peng, F. von Oppen, B. W. Heinrich, and K. J. Franke, *Phys. Rev. Lett.* **115**, 197204 (2015).
- [38] T.-P. Choy, J. M. Edge, A. R. Akhmerov, and C. W. J. Beenakker, *Phys. Rev. B* **84**, 195442 (2011).
- [39] S. Nadj-Perge, I. K. Drozdov, J. Li, H. Chen, S. Jeon, J. Seo, A. H. MacDonald, B. A. Bernevig, and A. Yazdani, *Science* **346**, 602 (2014).
- [40] S. Jeon, Y. Xie, J. Li, Z. Wang, B. A. Bernevig, and A. Yazdani, *Science* **358**, 772 (2017).
- [41] P. Marra and M. Nitta, *Phys. Rev. B* **100**, 220502 (2019).
- [42] R. Pawlak, S. Hoffman, J. Klinovaja, D. Loss, and E. Meyer, *Progress in Particle and Nuclear Physics* **107**, 1 (2019).
- [43] G. Górski, J. Baranski, I. Weymann, and T. Domanski, *Scientific Reports* **8**, 15717 (2018).
- [44] D. Crawford, E. Mascot, M. Shimizu, P. Beck, J. Wiebe, R. Wiesendanger, H. O. Jeschke, D. K. Morr, and S. Rachel, *npj Quantum Materials* **7**, 117 (2022).
- [45] L. Schneider, P. Beck, J. Neuhaus-Steinmetz, L. Rózsa, T. Posske, J. Wiebe, and R. Wiesendanger, *Nature Nanotechnology* **17**, 384 (2022).
- [46] M. Aghaee and *et al.*, *Nature* **638**, 651 (2025).
- [47] T. Dvir, G. Wang, N. van Loo, C.-X. Liu, G. P. Mazur, A. Bordin, S. L. D. ten Haaf, S. L. D. ten Haaf, J.-Y. Wang, D. van Driel, F. Zatelli, X. Li, F. K. Malinowski, S. Gazibegovic, G. Badawy, E. P. A. M. Bakkers, M. Wimmer, and L. P. Kouwenhoven, *Nature* **614**, 445 (2023).
- [48] S. L. D. ten Haaf, Q. Wang, A. M. Bozkurt, C.-X. Liu, I. Kulesh, P. Kim, D. Xiao, C. Thomas, M. J. Manfra, T. Dvir, M. Wimmer, and S. Goswami, *Nature* **630**, 329 (2024).
- [49] A. Bordin, C.-X. Liu, T. Dvir, F. Zatelli, S. L. D. ten Haaf, D. van Driel, G. Wang, N. van Loo, T. van Caekenberghe, J. C. Wolff, Y. Zhang, G. Badawy, S. Gazibegovic, E. P. A. M. Bakkers, M. Wimmer, L. P. Kouwenhoven, and G. P. Mazur, *Signatures of majorana protection in a three-site kitaev chain* (2024), [arXiv:2402.19382 \[cond-mat.supr-con\]](https://arxiv.org/abs/2402.19382).
- [50] J. D. Sau and S. D. Sarma, *Nature communications* **3**, 964 (2012).
- [51] M. Leijnse and K. Flensberg, *Phys. Rev. B* **86**, 134528 (2012).
- [52] A. Tsintzis, R. S. Souto, and M. Leijnse, *Phys. Rev. B* **106**, L201404 (2022).
- [53] A. Tsintzis, R. S. Souto, K. Flensberg, J. Danon, and M. Leijnse, *PRX Quantum* **5**, 010323 (2024).
- [54] R. S. Souto, A. Tsintzis, M. Leijnse, and J. Danon, *Phys. Rev. Res.* **5**, 043182 (2023).
- [55] M. Luethi, H. F. Legg, D. Loss, and J. Klinovaja, *Phys. Rev. B* **110**, 245412 (2024).
- [56] M. Luethi, H. F. Legg, D. Loss, and J. Klinovaja, *Phys. Rev. B* **111**, 115419 (2025).
- [57] M. Alvarado, A. L. Yeyati, R. Aguado, and R. S. Souto, *Phys. Rev. B* **110**, 245144 (2024).
- [58] D. Aasen, M. Hell, R. V. Mishmash, A. Higginbotham, J. Danon, M. Leijnse, T. S. Jespersen, J. A. Folk, C. M. Marcus, K. Flensberg, and J. Alicea, *Phys. Rev. X* **6**, 031016 (2016).
- [59] J. F. Steiner and F. von Oppen, *Phys. Rev. Res.* **2**, 033255 (2020).
- [60] M. I. K. Munk, J. Schulenburg, R. Egger, and K. Flensberg, *Phys. Rev. Res.* **2**, 033254 (2020).
- [61] D. Aasen and *et al.*, *Roadmap to fault tolerant quantum computation using topological qubit arrays* (2025), [arXiv:2502.12252 \[quant-ph\]](https://arxiv.org/abs/2502.12252).
- [62] M. Geier, R. S. Souto, J. Schulenburg, S. Asaad, M. Leijnse, and K. Flensberg, *Phys. Rev. Res.* **6**, 023281 (2024).
- [63] S. G. BRUSH, *Rev. Mod. Phys.* **39**, 883 (1967).
- [64] H. Bruus and K. Flensberg, *Many-Body Quantum Theory in Condensed Matter Physics* (Oxford: Oxford University Press) (2012).
- [65] D. Guerici and A. Nava, *Physica E: Low-dimensional Systems and Nanostructures* **134**, 114895 (2021).